DOI:10.1007/s41230-016-5126-7

Effect of Li on formation of long period stacking ordered phases and mechanical properties of Mg-Gd-Zn alloy

Li-yun Wei[1,2], *Jin-shan Zhang[1,2], Wei Liu[1,2], Chun-xiang Xu[1,2], Zhi-yong You[1,2], and Kai-bo Nie[1,2]

1. College of Materials Science and Engineering, Taiyuan University of Technology, Taiyuan 030024, China

2. Shanxi Key Laboratory of Advanced Magnesium-based Materials, Taiyuan 030024, China

Abstract: Alloys with composition of $Mg_{96-x}Gd_3Zn_1Li_x$ (at.%) (x=0, 2, 4, and 6) were prepared by conventional casting. The microstructures of these alloys under as-cast and solid-solution conditions have been observed, and the mechanical properties were investigated. The results showed that Li is an effective element to refine the grains and break the eutectic networks in as-cast $MgGd_3Zn_1$ alloy. During solid solution treatment, these broken eutectic networks are spheroidized and highly dispersed. In addition, plentiful lamellar long period stacking ordered (LPSO) phases are precipitated in an α-Mg matrix when the Li addition is not more than 4%. Solid-solution treated $Mg_{92}Gd_3Zn_1Li_4$ alloy exhibits an optimal ultimate tensile strength (UTS) of 226 MPa and elongation of 5.8%. The strength of $MgGd_3Zn_1$ alloy is improved significantly, meanwhile, the toughness is apparently increased.

Key words: Mg-Gd-Zn alloys; Li; second phase; long period stacking ordered phase; comprehensive properties

CLC numbers: TG146.22 **Document code:** A **Article ID:** 1672-6421(2016)04-256-06

Mg-Re-Zn alloys have attracted increasing attention due to their superior mechanical properties, attributing to the formation of lamellar long period stacking ordered (LPSO) phases within an α-Mg matrix [1-3]. Nevertheless, as a kind of second phase, the coarse block-like LPSO phase usually precipitates at grain boundaries during traditional solidification or subsequent solid solution treatment [4-5], which was reported to cause a decrease in strength [6-7]. Recently, various processes, such as extrusion [8-9], friction stir processing (FSP) [10-11] and severe plastic deformation [12-13], have been applied to achieve refined microstructure and enhanced mechanical properties. However, the coarse LPSO phase with excellent plasticity is hard to be broken. What's worse, all these methods will raise the production cost. Hence, there is a great importance to develop an effective and simple technology to decrease the detrimental influence of the coarse second phase.

Alloying treatment is a simple and economical method to improve the properties of alloys. To further improve the properties, heat treatment is usually adopted following the alloying treatment, which gives another simple and effective property improving method. Therefore, a proper combination of alloying and heat treatment is needed to obtain optimal mechanical properties. It has been demonstrated that Mn, Sr and Li are effective elements to modify the size and morphology of the second phases in cast aluminum alloys [14-16]. After heat treatment, the modified A380 aluminum alloy shows a significant improvement in tensile properties [17]. The method and principle of alloying and heat treatment for magnesium and aluminum alloys are similar. So, is it possible that the addition of these elements could modify the eutectic networks of as-cast Mg-Re-Zn alloy or turn the coarse second phase into less harmful forms during the following heat treatment?

Furthermore, the addition of Li can decrease the lattice constant ratios (c/a) through the substitution of Mg atoms by Li atoms, which will improve the ductility [18-20]. The reduction of the atomic distances causes a decrease in activation energy in the hcp crystal needed for prismatic slipping, as well as the dominating deformation over the basic plane [19]. In Mg-Re-Zn alloys, is it possible that the strength remains high by the formation of large amounts of LPSO phases; while the elongation is improved further by addition of Li? Up to date, few studies about

***Jin-shan Zhang**

Male, born in 1955, Professor. Research interests: strengthening and toughening of magnesium alloys.

E-mail: jinshansx@tom.com.

Received: 2015-12-22; Accepted: 2016-05-01

Li-containing Mg-Re-Zn alloys have been reported. In this study, Li was added to $MgGd_3Zn_1$ alloy, and the influences of Li on microstructures and mechanical properties of $MgGd_3Zn_1$ alloy were systematically studied.

1 Experimental procedure

$Mg_{96-x}Gd_3Zn_1Li_x$ alloys (at.%) (x=0, 2, 4, and 6) named as alloys A, B, C and D, respectively, were prepared by induction melting of high-purity Mg, Zn, Gd and Li in a mild steel crucible under a protective gas atmosphere of Ar. Pure Zn and Gd were added into the melt at 1,023 K after the melting of pure Mg, and held for 10 min. Then Li was added into the melt and held at 973 K for 10 min. Finally the melt was reheated to 1,003 K and poured into a cylindrical steel mold (Φ21 mm ×180 mm), which was preheated to 473 K. Solid solution treatment was performed at 773 K for 45 h in an OTF-1200X vacuum tube type furnace with a protective gas atmosphere of Ar, followed by furnace cooling.

The microstructures of as-cast and solid-solution treated alloys were investigated by optical microscopy (OM, Leica DM2500 M). The phase constitution was studied using X-ray diffraction (XRD) with monochromatic Cu-Kα radiation. The microstructures and compositions of different phases in alloys were analyzed using a field-emission scanning electron microscope (SEM, JUS-6700F) equipped with an energy dispersive X-ray spectrometry (EDS) and a transmission electron microscope (TEM, JEOL 2010). Tensile tests were performed using a DNS100 electronic universal material test machine with an initial strain rate of 3.33×10^{-4} s^{-1} at ambient temperature. Brinell hardness was measured using a HB-3000 Brinell hardness testing machine with a load of 62.5 kg and loading time of 30 s.

2 Results and discussion

2.1 Microstructures of as-cast alloys A, B, C and D

Figure 1 shows the optical microstructures (OM) of alloys A, B, C and D. White α-Mg and black eutectic structure phases at the grain boundary were observed in alloys with different addition amount of Li. According to the XRD patterns (Fig. 2) of the alloys A and C, the eutectic phases are confirmed as $(Mg,Zn)_3Gd$ phases, which is consistent with previous studies [4,5]. The morphologies of α-Mg grains and eutectic phases of the alloys change with different Li content. In Li-free alloy A, coarse dendrites were observed (Fig. 1a). After 2% Li was added, both the size of α-Mg grains and the amount of coarse dendrite decreased (Fig. 1b). When Li addition was up to 4%, both the size of α-Mg grains and coarse dendrites were further decreased (Fig. 1c). The 6% Li addition also could refine the α-Mg grains, meanwhile, it brought about a remarkable increase in the brittle eutectic phases (Fig. 1d).

The formation mechanism of $(Mg,Zn)_3Gd$ phase can be elucidated according to the Mg-Gd-Zn phase diagram [21]. The Mg-rich part in the liquidus projection of Mg-Gd-Zn system is shown in Fig. 3 [21]. It is clear that the composition points of the

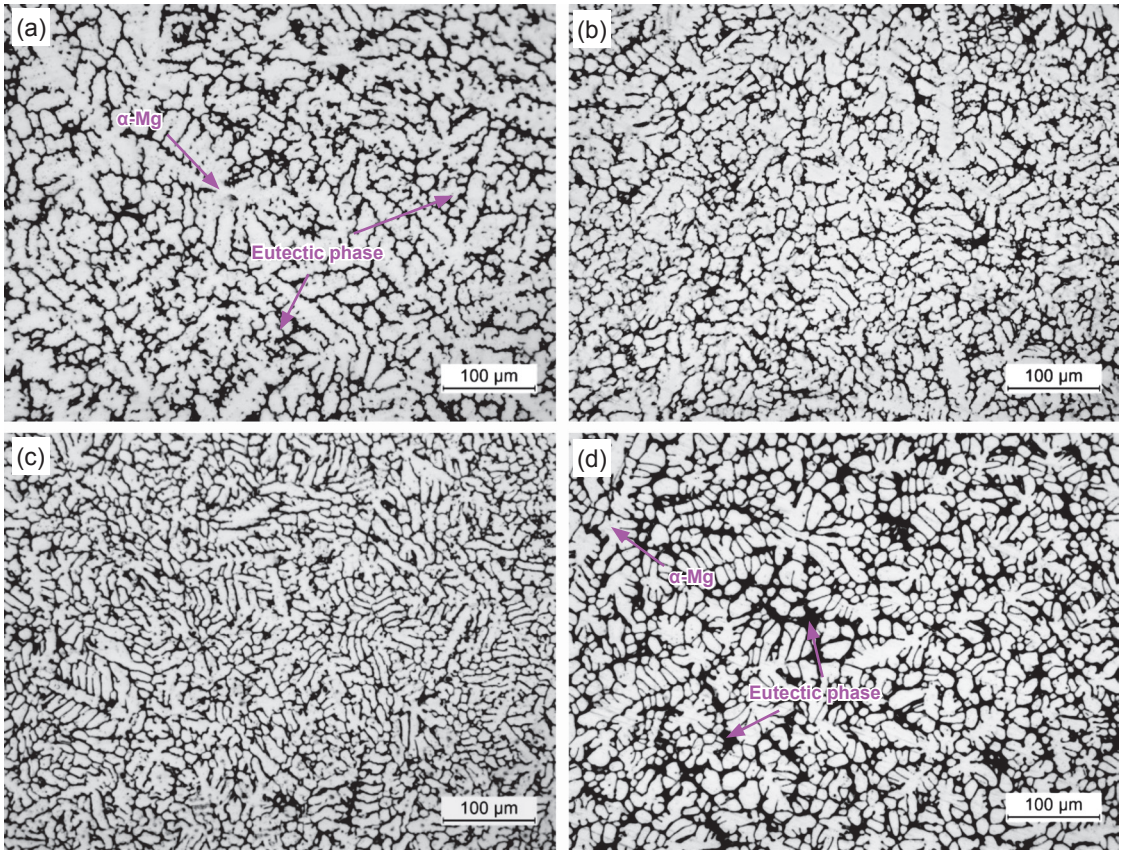

Fig. 1: OM images of as-cast alloy A (a), alloy B (b), alloy C (c), and alloy D (d)

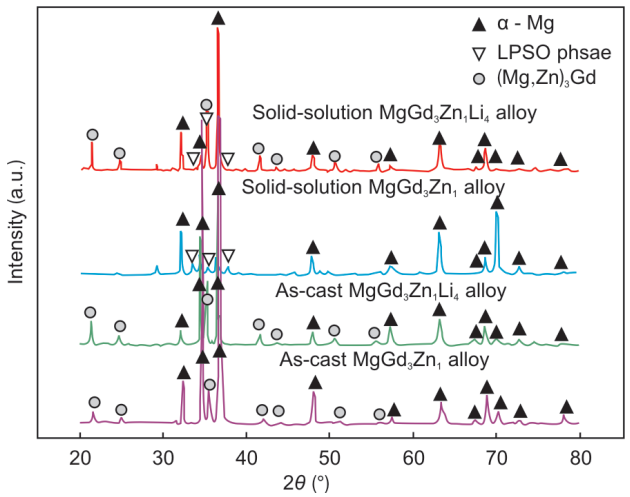

Fig. 2: XRD patterns of as-cast and solid-solution alloys A and C

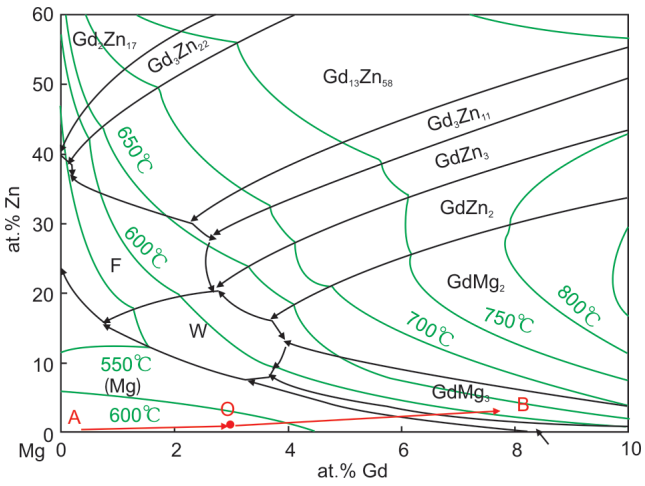

Fig. 3: Mg-rich part in the liquidus projection of Mg-Gd-Zn system [21]

samples we chose are located at point O. When crystallization starts, the composition of the liquid phase will move along the AO direction. However, it is impossible for Gd, Zn and Mg atoms to diffuse homogeneously under high cooling rates. So in the non-equilibrium freezing process, the composition of residual liquid contains a higher percentage of Gd and Zn elements than that in the equilibrium freezing process. That is to say the composition of the residual liquid reaches the point B where $(Mg,Zn)_3Gd$ phases crystallize first. Therefore, during the subsequent cooling and solidification, $(Mg,Zn)_3Gd$ rather than $(Mg,Zn)_5Gd$ phases crystallize until the end of the solidification.

The microstructures at higher magnification are shown in Fig. 4. It can be seen that the eutectic phases in Li-free alloy show continuous network morphology (Fig. 4a). The eutectic phases in Li-containing alloys present a chain continuous distribution, and some independent island and block-like eutectic phases can be found (Fig. 4b, alloy C). The changes above show that Li is an effective element to break the eutectic network. It can be inferred that the addition of Li may increase the liquidus temperature of the alloy and lower the eutectic reaction temperature, which is similar to the effect of Li on aluminum alloys [14-17, 22]. So a greater undercooling for eutectic reaction is needed in Li-containing alloys. The increased undercooling is considered to be the result of suppressed nucleation due to the eliminated nucleation sites. If there are fewer nucleation sites, it is harder for them to connect with each other during the following growth process and, therefore, a chain-like eutectic net is finally formed.

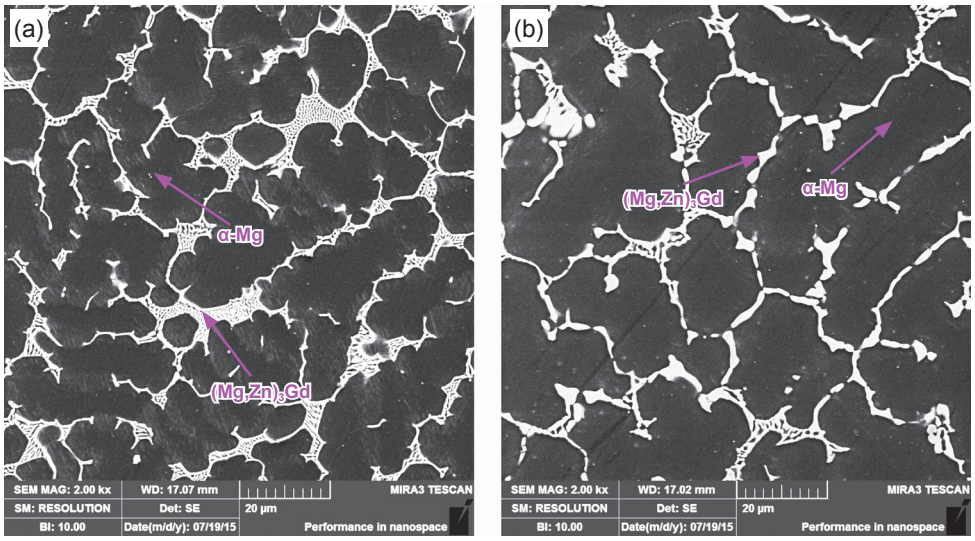

Fig. 4: SEM images of as-cast alloy A (a) and alloy C (b)

2.2 Microstructures of alloys A, B, C and D after solid solution treatment

Figure 5 shows SEM images of the alloys solid-solution treated at 773 K for 45 h. As shown in Fig. 5a, lamellar phases within the α-Mg matrix and coarse continuous phases at the grain boundaries were observed in the solid-solution treated alloy A. TEM bright field (BF) images and corresponding selected-area electron diffraction (SAED) patterns of coarse continuous phases and lamellar phases in solid-solution treated alloy A are shown in Fig. 6. In both SAED patterns, small periodic diffraction spots at the interval of 1/14 of distance between the direct spot and $(0002)_{Mg}$ reflection were observed, and the

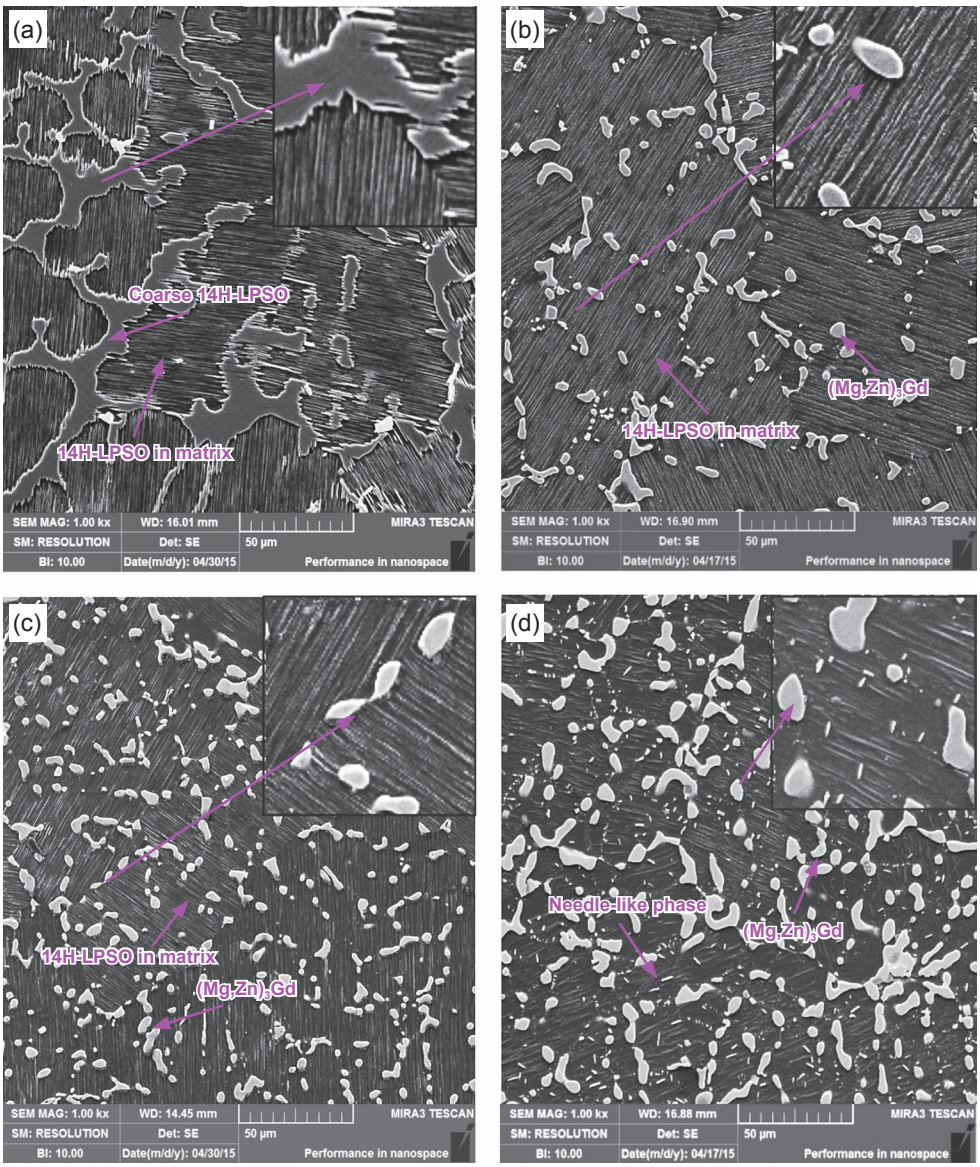

Fig. 5: SEM images of solid-solution treated alloys: (a) A, (b) B, (c) C, and (d) D

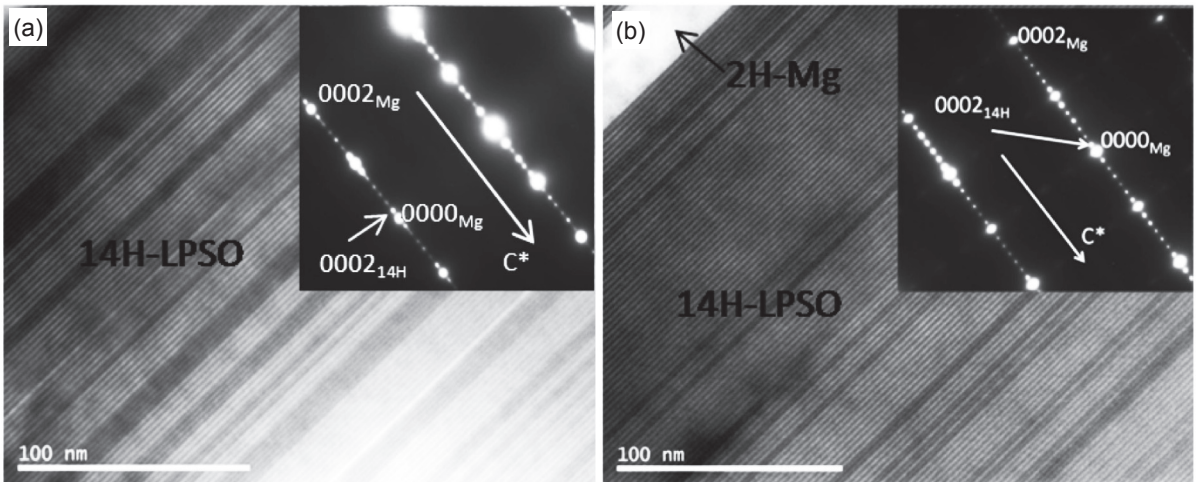

Fig. 6: BF images and corresponding SEAD patterns of (a) coarse continuous phases and (b) lamellar phases in solid-solution treated alloy A

spot of (0014) corresponded to that of $(0002)_{Mg}$. Based on the analyses mentioned above and the XRD peaks in Fig. 2, both the coarse continuous phase and lamellar phase were identified as 14H-LPSO structure phases, which were in agreement with previous investigations [4-5].

With the addition of Li, the microstructure of solid-solution

treated $MgGd_3Zn_1$ alloy changed significantly. On the one hand, there are no coarse continuous LPSO phases; but a lot of particle phases distributed in the α-matrix or at the grain boundaries were formed. According to XRD pattern (Fig. 2) of solid-solution treated alloy C, they were confirmed as $(Mg,Zn)_3Gd$ phases. During the none-equilibrium solidification process, Li is remarkably concentrated in the last solidification zone during the eutectic transformation, even in the alloy B which has the least Li addition. Li alloying can facilitate dislocation-mediated processes and tends to increase the stacking fault energy [23]. The LPSO phase may nucleate directly through stacking faults and the lower stacking fault energy is in favor of formation of the LPSO phase [24]. Moreover, these second phases with large amounts of Li may have higher thermal stability, which makes it hard for the diffusion of Mg, Gd and Zn atoms during solid solution treatment. In order to maintain the lowest system energy, the second phases spheroidized under the effect of surface energy during isothermal holding. In addition, the broken network second phases achieved under as-cast condition are beneficial to the spheroidization. Among the alloys containing Li in this study, the second phase particles of alloy C have both a smaller size on average and a more homogeneous distribution than the other two.

On the other hand, Li addition has an effect on lamellar LPSO phases within the Mg matrix. This effect is much weaker than that on coarse LPSO phases until the Li addition is more than 4%. In the cooling process of solid solution treatment, the 14H-LPSO phase mainly precipitates and grows from highly dispersed stacking faults [6]. When the Li addition is lower (alloys B and C), a smaller amount of Li solid dissolves in the matrix, which makes it harder to decrease the amount of stacking fault. Consequently, profuse 14H-LPSO phases are formed, as many as in the Li-free alloy form in the Mg matrix, as shown in Fig. 5a-c. However, Li has a strong suppressing effect on the formation of lamellar LPSO phases in the Mg matrix when the Li addition is more than 4%. As shown in Fig. 5d, alloy D is mainly composed of α-Mg matrix and $(Mg,Zn)_3Gd$ particles. In addition, a few loose lamellar structures and a large amount of highly dispersed needle-like precipitates were found in the α-Mg matrix. EDS result confirms the composition of these needle-like precipitates to be $MgGd_{10.4}Zn_{3.1}$. As the amount of Li solid dissolved in the α-Mg matrix increases, the stacking fault energy is increased greatly, which is too high to form profuse LPSO phases in the cooling process. Therefore, abundant Gd and Zn atoms precipitate from supersaturated α-Mg matrix in the form of needle-like precipitates instead of lamellar LPSO phases.

2.3 Mechanical properties of as-cast and solid-solution treated alloys A, B, C and D

The tensile stress-strain curves of alloys A, B, C and D under different conditions are shown in Fig. 7. It can be seen that with Li addition, the ultimate tensile strength (UTS) of as-cast alloy improved significantly and the elongation to failure (E_f) of as-cast alloys except alloy D increased as well. Although the grains have been refined by Li addition, there were still abundant brittle second phases at the grain boundaries in as-cast Li-containing alloys. Consequently, the E_f has not been improved significantly. Alloy C exhibits the highest strength and its UTS is 205 MPa, with an E_f of 4.3%, which is also the highest in as-cast alloys.

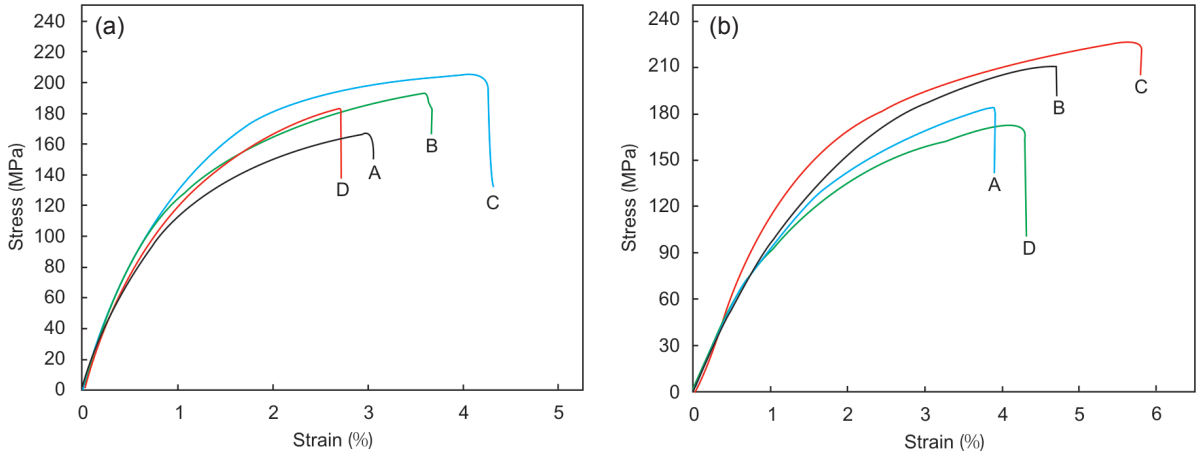

Fig. 7: Tensile stress-strain curves of (a) as-cast and (b) solid-solution treated alloys A, B, C and D

After solid solution treatment, the E_f of the four alloys was increased. Moreover, the UTS of all the alloys except D were also improved further. Alloy C, whose UTS was 226 MPa, with an E_f of 5.8%, exhibited the optimal strength and toughness in solid-solution treated alloys. The strengthening effects may result from multi-strengthening mechanisms, such as solid solution, profuse lamellar LPSO phases; and spheroidization and dispersion of second phases. Owing to the combined influence of Li addition and solid-solution treatment, abundant lamellar LPSO phases precipitated in the α-Mg matrix. Meanwhile, the second phases greatly spheroidized and dispersed. Lamellar LPSO phases can effectively hinder the movement of dislocation and thus enhance the strength of Mg alloys [25]. In addition, the coarse continuous second phases present in Li-free alloys were substituted by spheroidized and dispersed second phases after Li addition. So it can bear more loads transferred by the α-Mg grains during deformation. What's more, the lattice constant ratios were decreased by substitution of Mg atoms by Li atoms, which was favorable to the improvement of ductility. All these reasons above have led to an increase in the properties of Mg-Gd-Zn alloys.

3 Conclusions

(1) In as-cast $MgGd_3Zn_1$ alloy, Li was found to be effective in refining the grains and breaking the eutectic networks.

(2) Li addition could suppress the formation of LPSO phases during solid solution treatment of $MgGd_3Zn_1$ alloy. Coarse LPSO phases at the grain boundaries are suppressed significantly, while there is no obvious suppressing effect on the lamellar LPSO phases in the α-Mg matrix until the Li addition is more than 4%.

(3) After solid solution treatment on Li-containing $MgGd_3Zn_1$ alloys, spheroidized and dispersed second phases, rather than coarse continuous second phases are formed, which decreases the detrimental influence of coarse second phases.

(4) The coexistence of profuse lamellar LPSO phases and spheroidized and dispersed second phases leads to the optimal properties in solid-solution treated $MgGd_3Zn_1Li_4$ alloy with a UTS of 226 MPa and elongation of 5.8%. Both strength and toughness of $MgGd_3Zn_1$ alloy are improved significantly.

References

[1] Yamasaki M, Anan T, Yoshimoto S, et al. Mechanical properties of warm-extruded Mg-Zn-Gd alloy with coherent 14H long periodic stacking ordered structure precipitate. Scripta Materialia, 2005, 53(7): 799–803.

[2] Shao X H, Yang Z Q, and Ma X L. Strengthening and toughening mechanisms in Mg-Zn-Y alloy with a long period stacking ordered structure. Acta Materialia, 2010, 58(14): 4760–4771.

[3] Zhen R, Sun Y, Xue F, et al. Effect of heat treatment on the microstructures and mechanical properties of the extruded Mg–11Gd–1Zn alloy. Journal of Alloys and Compounds, 2013, 550: 273–278.

[4] Zhang J, Zhang W, Bian L, et al. Study of Mg-Gd-Zn-Zr alloys with long period stacking ordered structures. Materials Science and Engineering: A, 2013, 585: 268–276.

[5] Wu Y J, Zeng X, Lin D L, et al. The microstructure evolution with lamellar 14H-type LPSO structure in an $Mg_{96.5}Gd_{2.5}Zn_1$ alloy during solid solution heat treatment at 773 K. Journal of Alloys and Compounds, 2009, 477(1): 193–197.

[6] Yamasaki M, Sasaki M, Nishijima M, et al. Formation of 14H long period stacking ordered structure and profuse stacking faults in Mg-Zn-Gd alloys during isothermal aging at high temperature. Acta Materialia, 2007, 55(20): 6798–6805.

[7] Lu F M, Ma A B, Jiang J H, et al. Formation of profuse long period stacking ordered microcells in Mg-Gd-Zn-Zr alloy during multipass ECAP process. Journal of Alloys and Compounds, 2014, 601: 140–145.

[8] Wu Y J, Peng L M, Zeng X Q, et al. A high-strength extruded Mg-Gd-Zn-Zr alloy with super-plasticity. Journal of Materials Research, 2009, 24(12): 3596–3602.

[9] Yamasaki M, Hashimoto K, Hagihara K, et al. Effect of multimodal microstructure evolution on mechanical properties of Mg-Zn-Y extruded alloy. Acta Materialia, 2011, 59(9): 3646–3658.

[10] Li X W, Zheng F Y, Wu Y J, et al. Modification of long period stacking ordered phase and improvement of mechanical properties of Mg-Gd-Zn-Zr alloy by friction stir processing. Materials Letters, 2013, 113: 206–209.

[11] Yang Q, Xiao B L, Wang D, et al. Study on distribution of long-period stacking ordered phase in Mg-Gd-Y-Zn-Zr alloy using friction stir processing. Materials Science and Engineering: A, 2015, 626: 275–285.

[12] Xiao H C, Jiang S N, Tang B, et al. Hot deformation and dynamic re-crystallization behaviors of Mg-Gd-Y-Zr alloy. Materials Science and Engineering: A, 2015, 628: 311–318.

[13] Tahreen N, Zhang D F, Pan F S, et al. Characterization of hot deformation behavior of an extruded Mg-Zn-Mn-Y alloy containing LPSO phase. Journal of Alloys and Compounds, 2015, 644: 814–823.

[14] Ashtari P, Tezuka H, and Sato T. Influence of Li addition on inter-metallic compound morphologies in Al-Si-Cu-Fe cast alloys. Scripta Materialia, 2004, 51(1): 43–46.

[15] Hwang J Y, Doty H W, and Kaufman M J. The effects of Mn additions on the microstructure and mechanical properties of Al-Si-Cu casting alloys. Materials Science and Engineering: A, 2008, 488(1): 496–504.

[16] Azarbarmas M, Emamy M, and Alipour M. Microstructure, hardness and tensile properties of A380 aluminum alloy with and without Li additions. Materials Science and Engineering: A, 2013, 582: 409–414.

[17] Karamouz M, Azarbarmas M, and Emamy M. On the conjoint influence of heat treatment and lithium content on microstructure and mechanical properties of A380 aluminum alloy. Materials & Design, 2014, 59: 377–382.

[18] Drits M E, Elkin F M, and Gur'ev I I. Magnesium-Lithium Alloys. Metallurgia, Moscow, 1980.

[19] Haferkamp H, Boehm R, Holzkamp U, et al. Platform Science and Technology for Advanced Magnesium Alloys, Alloy Development, Processing and Applications in Magnesium Lithium Alloys. Materials Transactions, 2001, 42(7): 1160–1166.

[20] Yang C W and Chen Y W. Effects of Artificial Aging and Precipitation on Tensile Mechanical Properties and Failure Mechanism of the Friction Stir Processed Dual-phase Mg-Li Alloy. Procedia Engineering, 2014, 75: 88–92.

[21] Gröbner J, Kozlov A, Fang X Y, et al. Phase equilibria and transformations in ternary Mg-Gd-Zn alloys. Acta Materialia, 2015, 90: 400–416.

[22] Pan Y, Yang H, Liu X, et al. Effect of K/Na on microstructure of high-speed steel used for rolls. Materials Letters, 2004, 58(12): 1912–1916.

[23] Han J, Su X M, Jin Z H, et al. Basal-plane stacking-fault energies of Mg: A first-principles study of Li- and Al-alloying effects. Scripta Materialia, 2011, 64(8): 693–696.

[24] Pan F, Luo S, Tang A, et al. Influence of stacking fault energy on formation of long period stacking ordered structures in Mg-Zn-Y-Zr alloys. Progress in Natural Science: Materials International, 2011, 21(6): 485–490.

[25] Huang S, Wang J, Hou F, et al. Effect of Gd and Y contents on the microstructure evolution of long period stacking ordered phase and the corresponding mechanical properties in Mg-Gd-Y-Zn-Mn alloys. Materials Science and Engineering: A, 2014, 612: 363–370.

This work was supported by the National Natural Science Foundation of China (Nos. 50571073, 51574175 and 51474153): the Ph.D. Programs Foundation of Ministry of Education of China (20111402110004): and the Natural Science Foundation of Shanxi Province (Nos. 2009011028-3 and 2012011022-1).